Elemental analysis by microwave-assisted laser-induced breakdown spectroscopy: Evaluation on ceramics

Yuan Liu, Matthieu Baudelet* and Martin Richardson

Received 17th February 2010, Accepted 5th May 2010
DOI: 10.1039/c003304a

A new Laser-Induced Breakdown Spectroscopy (LIBS) enhancement method utilizing interaction between microwave radiation and laser-induced plasma has been evaluated. Experimental parameters such as laser pulse irradiance, microwave duration, and surrounding gas were studied and optimized for the microwave effect through a series of experiments on a piece of alumina ceramic sample. Up to 33 times enhancement on different spectral lines was achieved. Enhancement of the line intensity was found to be at a maximum when the laser ablation was induced at low irradiance on a large area in normal atmosphere. The enhancement was element-dependent and stronger for transitions with low excitation energy. The microwave enhancement in argon atmosphere was not as effective as in air, and the reasons are discussed.

Introduction

Atomic emission spectroscopy (AES) techniques utilize a radiation source to produce free atoms, excite levels with high emission efficiency, and eventually ionize the species to provide ionic emitters.[1,2] These sources are usually flames or plasmas: arcs, sparks, plasma jets, inductively coupled plasma (ICP), high-frequency plasma, microwave plasma, glow discharges, laser-induced plasma.[1,3] Laser-induced plasma emission spectroscopy, or Laser-Induced Breakdown Spectroscopy (LIBS), has multiple advantages for being an efficient analytical AES technique. A typical LIBS setup includes a laser system, focusing optics to concentrate the laser intensity onto the sample and create a plasma, collection optics (free space or fiber-based) coupled to a spectrometer with detector to collect the plasma emission and record spectra, and a computer for spectrum analysis. These instruments are generally easy to use, so operating a LIBS system does not require highly specialized personnel training. The main advantage in LIBS is the simultaneous sampling and excitation that can be achieved with a single laser pulse. Many solid samples can be analyzed directly or with minimal preparation, so LIBS shortens the full analysis cycle compared to most other analysis techniques. Standard ICP or discharge based techniques must use background argon or other noble gases to perform analysis, which is not a necessary part for most LIBS experiments.

Although LIBS is considered a promising analysis technique for various industrial, civilian, and military applications,[4–10] there are aspects in which LIBS cannot match the standard ICP techniques, such as the limits of detection, and reproducibility. In order to improve the overall performance of LIBS, double pulse LIBS has been studied extensively.[11–14] Different configurations have been investigated: in collinear or orthogonal geometry, the first pulse being either a pre-ablation pulse, to prepare the sample or the atmosphere above the sample, or the ablation pulse, and the second, being respectively, the ablation pulse or a heating pulse.[11] For the configuration that induces the plasma with the first pulse and controls plasma emission lifetime with the second one, emission enhancement up to several hundred times has been observed.[15] However, for many applications, adding another laser system increases the cost and further complicates the setup. Similar improvements have been made but without the use of an additional laser. Recent works have utilized other radiations for controlling the plasma in the microwave spectral region. Ikeda and Kaneko[16] used microwaves to heat laser- or spark-induced air plasmas and sustain the emission to milliseconds range. Ocean Optics demonstrated the signal enhancement ability of their LAMPS (Laser-Assisted Microwave Plasma Spectroscopy) system, which also utilizes microwave plasma interaction.[17] Envimetrics[18] and Liu *et al.*[19] reported signal enhancement effect using microwave plasma coupling on metal samples such as aluminium and lead. Replacing the second laser in a double pulse LIBS setup with a commercially available microwave system could potentially reduce the cost and complexity, while maintain the performance. Moreover, the microwave plasma interaction shows possibility to generate controllable plasma as discussed in the following paragraph.

The principle behind Microwave-Assisted LIBS (MA-LIBS) relies on the coupling of microwave radiation in the low electron density regions of the plasma thanks to a critical electron density N^e_{cr} on the order of 10^{11} cm^{-3} (7.10^{10} cm^{-3} for a radiation at 2.45 GHz). Initially the plasma has a high electron density (about 10^{17}–10^{19} cm^{-3}) but during its relaxation and at its periphery, this density decreases below N^e_{cr}. The plasma is then no longer a mirror for the microwave radiation and can be coupled to the electromagnetic field. Rapid decrease of the electron density will stop at this moment, because the microwave field can then drive the motion of the free electrons and provide them with kinetic energy to excite the de-excited atoms and ions by multiple electron-atom/ion collision. Since excited atoms and ions in the plasma are useful emitters which give characteristic line emission of the constituent elements, more emission contributing to the

Townes Laser Institute, CREOL-The College of Optics and Photonics, University of Central Florida, Orlando, FL, 32816, USA. E-mail: baudelet@creol.ucf.edu

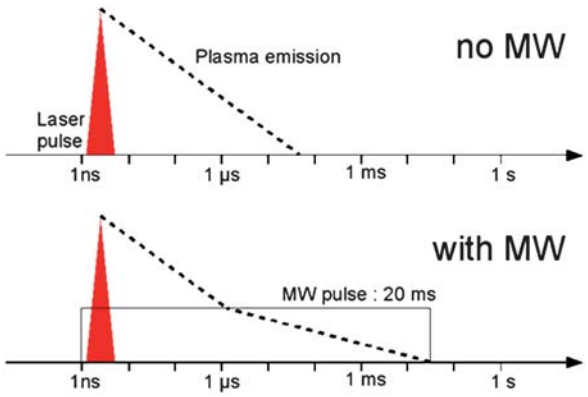

Fig. 1 Principles of Microwave-Assisted LIBS. Plasma emission decreases fast without microwave (above); plasma emission lasts milliseconds due to microwave plasma coupling, when electron density drops below N^e_{cr} (below).

useful signal is expected to be detected. As long as the microwave is coupled, energy can be transferred to the plasma, and the emission lifetime of the plasma could potentially be the microwave duration. As a consequence, the emission from the constituents of the plasma is enhanced due to larger integration time, by comparison with a non-coupled system as shown in Fig. 1.

In this paper, the analytical ability of Microwave-Assisted Laser-Induced Breakdown Spectroscopy (MA-LIBS) on a relatively complex alumina sample is systematically studied for the first time. The questions we try to answer are:

- What are the best experimental parameters of the MA-LIBS system to perform chemical analysis?
- Is the enhancement effective for all elements?
- What is the influence of different ionization stages and energy levels?
- Does the atmosphere have an influence on the enhancement effect?

Experimental

The experimental setup is illustrated in Fig. 2. It consisted in a typical LIBS setup with the addition of a focusing microwave cavity above the sample to control the expansion of the plasma.

Ablation system

A Nd:YAG laser (Brilliant, Quantel) with 5 ns pulse duration at 1064 nm was used with a 10 cm focal length lens with anti-reflection coating as the ablation source. The maximum pulse energy of the laser was 300 mJ, but the combination of a half-wave plate and a polarizer cube controlled the actual laser energy on the sample (from 1.5 mJ to 61 mJ in our study). As an additional degree of freedom, a translation stage could adjust the lens-to-sample distance around the focal position, controlling the area of the focusing spot, and as a consequence, the irradiance of the laser. The beam diameter, which was obtained from a knife-edge scan measurement, varied from about 100 µm near focal point to 1200 µm at the maximum defocusing available.

The samples were placed outside the microwave cavity but close to its bottom aperture where the electromagnetic field was the strongest. An X–Y translation stage was used in order to provide a pristine surface for each laser shot during the analysis. The cavity and the sample could be enclosed by a plastic bag for the control of the atmosphere above the sample, allowing the plasma to expand either in normal atmosphere or in argon, both at room temperature and atmospheric pressure.

Microwave cavity

The microwave system was designed and manufactured by Envimetrics. It consisted of a 2.45 GHz magnetron generating 1 kW pulsed microwave with tunable duration from less than 1 ms to 28 ms. The power of the microwave pulse was not controllable and set to 1000 W. The microwave pulse was guided to a focusing cavity, in which the maximum intensity was close to the bottom aperture, also where the sample was positioned. The

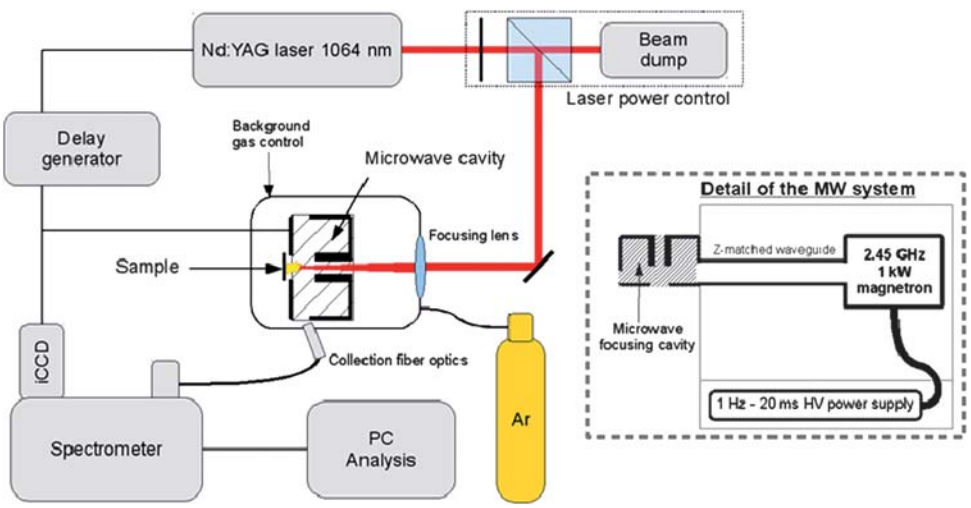

Fig. 2 Experimental setup. A microwave cavity was added to a typical LIBS system between the focusing lens and the sample. Plasma expands into the microwave cavity and gets coupled with microwave to achieve signal enhancement.

Table 1 Alumina sample chemical composition

Atomic species (form in the sample)	Weight percentage of the atomic species from XRF (commercial data sheet)
Aluminium (Al_2O_3)	42.74 ± 0.14 (47.37)
Oxygen (oxides)	53.29 ± 0.16 (46.91)
Silicon (SiO_2)	0.82 ± 0.04 (3.04)
Magnesium (MgO)	1.31 ± 0.04 (1.45)
Calcium (CaO)	0.18 ± 0.02 (0.54)
Baryum (BaO)	–(0.45)
Iron (Fe_2O_3)	0.16 ± 0.04 (0.1)
Sodium (Na_2O)	0.15 ± 0.03 (0.09)
Titanium (TiO_2)	0.10 ± 0.03 (0.03)
Potassium (K_2O)	–(0.02)
Phosphorus (–)	0.52 ± 0.03 (–)
Silver (–)	0.71 ± 0.06 (–)

whole system had a power leakage lower than the microwave oven safety standards.[18]

Detection optics and spectral acquisition

The plasma emission was collected directly with a UV-transmissive multi-mode optical fiber with a numerical aperture of 0.22.

Plasma emission was transported to a 0.3 m Czerny–Turner spectrometer (2300i, Princeton Instruments – Acton) equipped with a 1800 l mm^{-1} grating. A 512 × 512 pixels UV-sensitive GenII iCCD camera (PIMAX, Princeton Instruments) was used for the study providing a resolution from 0.02 to 0.04 nm/pixel depending on the wavelength.

The whole timing configuration of the setup was driven by a delay generator (DG645, Stanford Research Systems) controlled the firing of the laser (*via* the Q-switch), and the injection of the microwave cavity. The inter-pulse delay between the microwave and the laser did not show a noticeable effect on the spectral intensity or stability as long as the microwave and the plasma have enough overlap in time. 20 μs were needed to stabilize the microwave signal, so the microwave pulse was triggered 25 μs before the laser pulse. The acquisition by the iCCD camera was delayed by 1 μs after the ablation by the laser and lasted 30 μs when the microwave cavity was not activated, and as long as the microwave pulse duration when it was activated. Each spectrum was obtained by averaging ten single shot spectra on a fresh surface.

Samples

The ceramic sample was an alumina plate (AD-90-S2, CoorsTek). Table 1 shows the composition of the sample listed by the vendor and measured by X-Ray fluorescence measurement. Differences can be noticed between the two analyses: barium and potassium were not detected by the XRF analysis whereas silver and phosphorus are not listed in the data sheet, but appeared in the XRF measurements.

Results and discussion

Choice of spectral lines

A high resolution LIBS spectrum of the alumina sample from 200 nm to 790 nm shown in Fig. 3 was obtained by connecting 24 individual spectra to cover the whole spectral region of our detection system. Each individual spectrum was recorded by a second 1024 × 512 pixel camera with a laser power of 5 MW on a 1 mm diameter spot (irradiance of 640 MW cm^{-2}) and microwave pulse duration of 20 ms. The experimental parameters mentioned above were empirically optimized for best enhancement as explained later in the text. Line 1 shows the MA-LIBS spectrum while line 2 is for traditional LIBS. Distinct enhancement effect of Al, Mg, Ca, and Na emission lines can be observed from this comparison. However, enhanced molecular electronic emission, from oxides formed in the plasma or with interaction with the atmospheric oxygen, was visible: AlO ($B^2\Sigma^+ \rightarrow X^2\Sigma^+$), NO ($A^2\Sigma^+ \rightarrow X^2\Pi$) and OH ($A^2\Sigma^+_{v=0} \rightarrow X^2\Pi_{v=0}$). In addition, second order diffraction lines were also detected for the four elements with the larger concentrations (Al, Si, Mg, Ca which

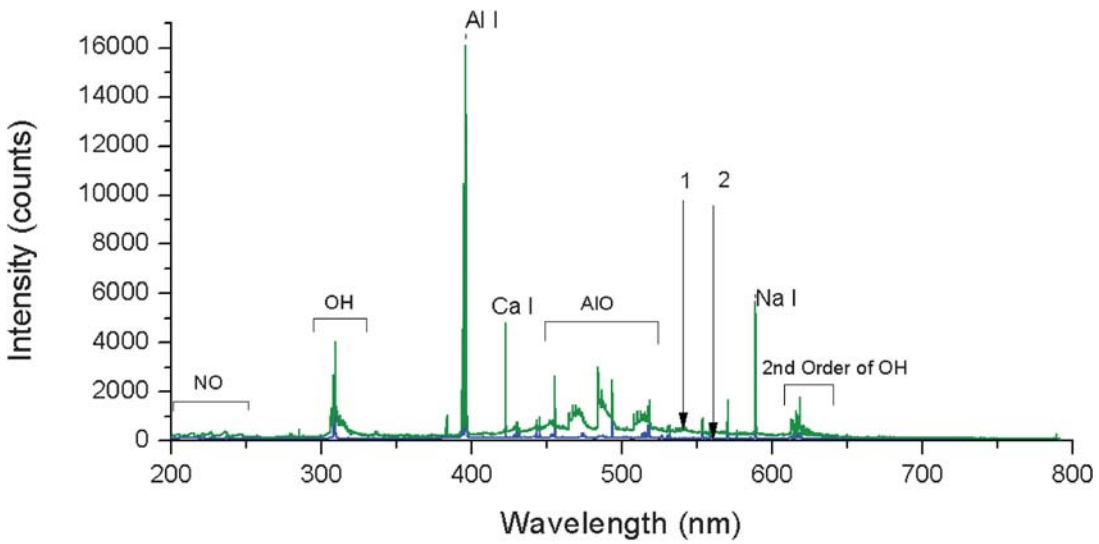

Fig. 3 Alumina spectra from 200 nm to 790 nm. (1: MA-LIBS signal, 2: traditional LIBS signal).

Table 2 Summary of spectral lines from Fig. 3.[b]

λ/nm Al I	λ_{NIST}/nm	E_{up}/eV	E_{low}/eV	Configuration	A_{ki}/s^{-1}	g_k	g_i
220.513	220.466	5.62196	0	$3s^23p–3s^26d$	4.53E+07	4	2
220.944	221.0046	5.622137	0.013894	$3s^23p–3s^26d$	5.40E+07	6	4
226.235	226.3462	5.475935	0	$3s^23p–3s^25d$	6.60E+07	4	2
226.883	226.9096	5.476239	0.013894	$3s^23p–3s^25d$	7.90E+07	6	4
236.667	236.7052	5.236316	0	$3s^23p–3s^24d$	7.20E+07	4	2
237.278	237.3124	5.236817	0.013894	$3s^23p–3s^24d$	8.60E+07	6	4
256.889	256.7984	4.826632	0	$3s^23p–3s^2(^1S)$nd	2.30E+07	4	2
257.532	257.5094	4.827197	0.013894	$3s^23p–3s^2(^1S)$nd	2.80E+07	6	4
265.287	265.2484	4.672891	0	$3s^23p–3s^25s$	1.33E+07	2	2
266.092	266.0393	4.672891	0.013894	$3s^23p–3s^25s$	2.64E+07	4	2
308.241	308.2153	4.021483	0	$3s^23p–3s^23d$	6.30E+07	4	2
309.31	309.271	4.02165	0.013894	$3s^23p–3s^23d$	7.40E+07	6	4
394.471	**394.4006**	**3.142721**	**0**	**$3s^23p–3s^24s$**	**4.93E+07**	**2**	**2**
396.221	**396.152**	**3.142721**	**0.013894**	**$3s^23p–3s^24s$**	**9.80E+07**	**2**	**4**
Si I							
288.168	288.1579	5.082346	0.780958	$3s^23p^2–3s^23p4s$	1.89E+08	3	5
Mg I							
278.17[a]				$3s3p–3p^2$			
285.22	**285.2127**	**4.345803**	**0**	**$2p^63s^2–3s3p$**	**4.91E+08**	**3**	**1**
383.251	383.2304	5.945913	2.711592	$3s3p–3s3d$	1.21E+08	5	3
383.805	383.8292	5.945915	2.71664	$3s3p–3s3d$	1.61E+08	7	5
516.847	516.7322	5.107827	2.709105	$3s3p–3s4s$	1.13E+07	3	1
517.406	517.2684	5.107827	2.711592	$3s3p–3s4s$	3.37E+07	3	3
518.487	518.3604	5.107827	2.71664	$3s3p–3s4s$	5.61E+07	3	5
Mg II							
279.635	**279.5528**	**4.433784**	**0**	**$2p^63s–2p^63p$**	**2.60E+08**	**4**	**2**
280.262	**280.2704**	**4.422431**	**0**	**$2p^63s–2p^63p$**	**2.57E+08**	**2**	**2**
Ca I							
422.734	**422.673**	**2.932512**	**0**	**$3p^64s^2–3p^64s4p$**	**2.18E+08**	**3**	**1**
428.432	**428.301**	**4.779784**	**1.885807**	**$3p^64s4p–3p^64p^2$**	**4.34E+07**	**5**	**3**
429.037	428.936	4.769028	1.87934	$3p^64s4p–3p^64p^2$	6.00E+07	3	1
430.018	429.899	4.769028	1.885807	$3p^64s4p–3p^64p^2$	4.66E+07	3	3
430.32	430.253	4.779784	1.898935	$3p^64s4p–3p^64p^2$	1.36E+08	5	5
430.848	430.774	4.763168	1.885807	$3p^64s4p–3p^64p^2$	1.99E+08	1	3
431.977	431.865	4.769028	1.898935	$3p^64s4p–3p^64p^2$	7.40E+07	3	5
442.529	442.544	4.68018	1.87934	$3p^64s4p–3p^64s4d$	4.98E+07	3	1
443.513	443.569	4.68018	1.885807	$3p^64s4p–3p^64s4d$	3.42E+07	3	3
445.513	443.589	4.680635	1.898935	$3p^64s4p–3p^64s4d$	2.00E+07	5	5
Ca II							
393.419	393.366	3.150984	0	$3p^64s–3p^64p$	1.47E+08	4	2
396.92	396.847	3.123349	0	$3p^64s–3p^64p$	1.40E+08	2	2
Ba I							
553.729	**553.5481**	**2.239187**	**0**	**$6s^2–6s6p$**	**1.19E+08**	**3**	**1**
614.39	614.1713	2.721751	0.703586	$5d–6p$	4.12E+07	4	6
Ba II							
455.492	**455.4033**	**2.721751**	**0**	**$6s–6p$**	**1.11E+08**	**4**	**2**
493.553	493.4077	2.512113	0	$6s–6p$	9.53E+07	2	2
Fe I							
407.725	407.6629	6.251672	3.211189	$3p^63d^6(^5D)4s4p(^3P^0)–3p^63d^6(^5D)4s(^6D)4d$	1.90E+07	9	9
413.126	413.2058	4.607592	1.607895	$3p^63d^7(^4F)4s–3p^63d^7(^4F)4p$	1.20E+07	7	5

Na I							
588.937	588.995	2.104429	0	$2p^6 3s–2p^6 3p$	6.16E+07	4	2
589.532	**589.5924**	**2.102297**	**0**	**$2p^6 3s–2p^6 3p$**	**6.14E+07**	**2**	**2**
Ti I							
475.774	475.812	4.854236	2.249226	$3d^3(^2H)4s–3d^3(^2H)4p$	7.13E+07	11	11
K I							
766.21	**766.49**	**1.61711**	**0**	**$3p^6 4s–3p^6 4p$**	**3.87E+07**	**4**	**2**

[a] Multiple lines. [b] Spectral lines in bold rows are characteristic emission lines for our study.

have strong emission lines below 395 nm) throughout the spectrum, which may cause line interference with the emission lines from low probability transitions. Even though oxygen has a large concentration in the sample (54% wt), its emission was not visible in the spectrum shown in Fig. 3 because of the low irradiance although the emission lines around 777 nm ($2s^2 2p^3(^4S^0)3s$-$2s^2 2p^3(^4S^0)3p$ multiplet) were detected, when the sample was positioned at the focal plane of the focusing lens.

Emission lines of all the elements listed in the commercial data sheet can be found. A summary of the spectral lines is shown in Table 2. The 422.7 nm atomic calcium emission line ($3p^6 4s^2$–$3p^6 4s4p$) was chosen to further study the analytical performance of the MA-LIBS system, because calcium could be a representative of minor constituent of the sample (0.18% wt), and this particular line did not interfere with other transition lines in the spectrum and it was subject to significant enhancement by the microwave radiation.

Influence of different parameters in the setup

Laser irradiance. The relationship between laser irradiance on the sample surface and the MA-LIBS enhancement was studied. The irradiance was controlled in two ways: either by changing the laser energy with the sample at the focal plane of the focusing lens or by changing the diameter of the laser spot size by defocusing the laser beam. Fig. 4 shows the intensity of the Ca I line as a function of the laser irradiance with the sample surface at focus without microwave radiation. Two regions can be outlined: below and above 50 GW cm^{-2}. The first region shows an efficient ablation (increase of the signal with the laser irradiance). The second region shows a screening effect, where the tail of the laser pulse is reflected by the high electron density plasma at early times (first nanoseconds) created by the high irradiance ablation.[20] The uncontrolled interaction between the tail of the laser pulse and the expanding plasma increases the fluctuations from shot to shot, depicted by the large standard deviations on the figure. Laser energies of 1.5, 6, 14, 25, and 47 mJ were used as test values to characterize the effect of the laser pulse irradiance across the behavior shown in Fig. 4.

Fig. 5 shows the enhancement factor as a function of the area of the ablation spot (negative spot size means that the laser is focused inside the sample.) for different laser peak powers. The enhancement was defined as the ratio between the MA-LIBS intensity and LIBS intensity after baseline removal. To vary the area of the ablation spot, the laser beam was focused down to 2.2 cm, 1.4 cm, 1 cm, 0.1 cm inside the sample and 0.7 cm above the sample surface. After defocusing, the plasma emission was either undetectably weak or very unstable if the laser energy was 1.5 mJ or 6 mJ. This corresponded to an irradiance smaller than 250 MW cm^{-2}, which is approximately the plasma threshold for alumina.[15] Low energy and large defocusing, leading to low irradiance ablation, benefited MA-LIBS enhancement, as it can be seen clearly from the enhancement graph shown in Fig. 5. These characteristics result from two aspects. First, high irradiance laser ablation generates plasma with high electron density. Thus, when the plasma expands into the microwave cavity, the

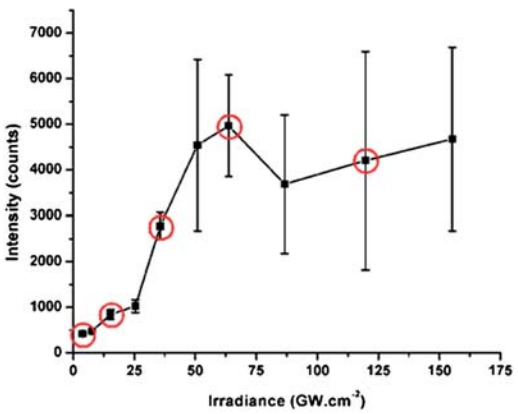

Fig. 4 Ca I line at 422.7 nm intensity *vs.* laser irradiance.

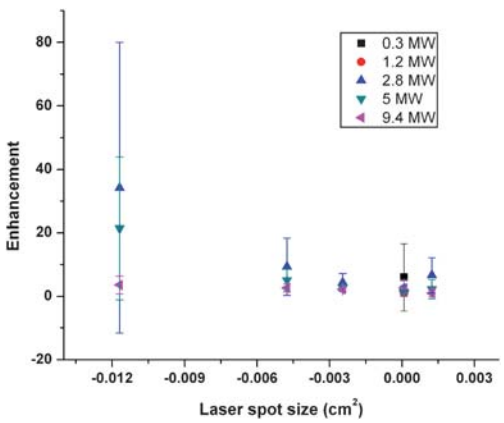

Fig. 5 Enhancement dependence on laser power and laser spot size in air.

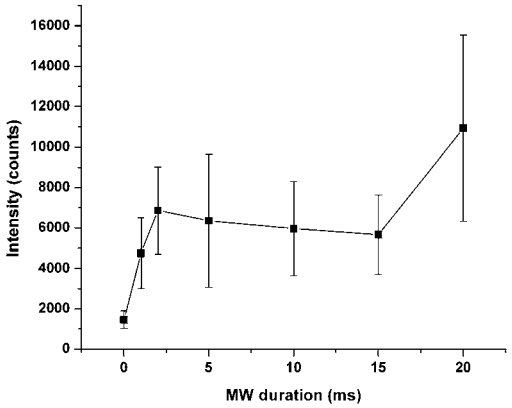

Fig. 6 422.7 nm Ca I line intensity as a function of the microwave pulse duration.

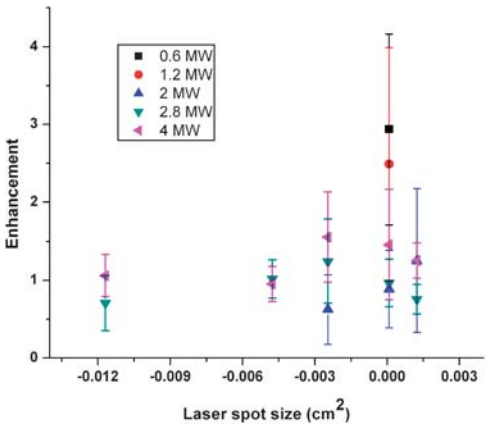

Fig. 7 Microwave enhancement *vs.* laser power and spot size in Ar.

impedance of the cavity is modified. Impedance mismatch leads to more microwave reflection, and hence lowers the energy coupled to the plasma. Second, a corollary to this explanation is that low irradiance ablation produces low electronic density plasma that reaches the critical electron density for coupling faster than that created at high irradiance. Therefore the enhancement went up when laser energy dropped. From Fig. 5 we can see that the enhancement was very weak at the focus whatever the laser irradiance was. This is because defocusing helps to create large and uniform laser plasma with relatively low electron density, which can couple more efficiently with the microwave radiation. However, focusing the laser beam in front of the sample surface is likely to cause air plasma, and hence degrade the quality of the spectrum. As a consequence, defocusing of the ablation process is critically important in order to achieve good enhancement factors. This feature indicates the possibility to use compact low peak power lasers in MA–LIBS systems without losing plasma emission.

Microwave pulse duration. The influence of the microwave pulse duration was examined. In order to avoid comparison of null or very low intensity values, 5 MW laser pulses were used with a 2.2 cm defocusing. The 422.7 nm Ca I intensity with microwave assistance is illustrated in Fig. 6. For MW pulses below 3 ms, the spectral emission intensity increases with pulse duration, showing an efficient coupling between the plasma and the microwave radiation. For longer pulses, the intensity remains relatively constant, denoting that the microwave radiation is no longer coupled after 3 ms. The larger mean value for pulses of 20 ms seems not representative of any effect because of the large standard deviation of the signal.

Atmospheric background. The next factor important to the MA-LIBS performance is the atmosphere composition above the sample. All previous experiments were carried out in air. As mentioned above, the presence of air and its interaction with the plasma led to molecular formation (AlO, NO, OH). Molecular band emission produced background signal that overlapped with the atomic emission and introduces its own fluctuation to the noise in the emission spectrum. To study the effect of the atmosphere, we purged the microwave cavity with argon gas and optimized experimental parameters the same way as in the air. In an argon environment, the microwave enhancement effect behaved differently from in the air as illustrated in Fig. 7. Weak enhancement can be observed at focus, but no enhancement with optimized experimental parameter found in the air (laser power below 5 MW, large ablation spot area—0.012 cm^2—and long microwave pulse—20 ms). With all the parameters tested, the enhancement is negligible compared (up to 4) with the results in the air. Fig. 8a shows the spectrum for the calcium emission in

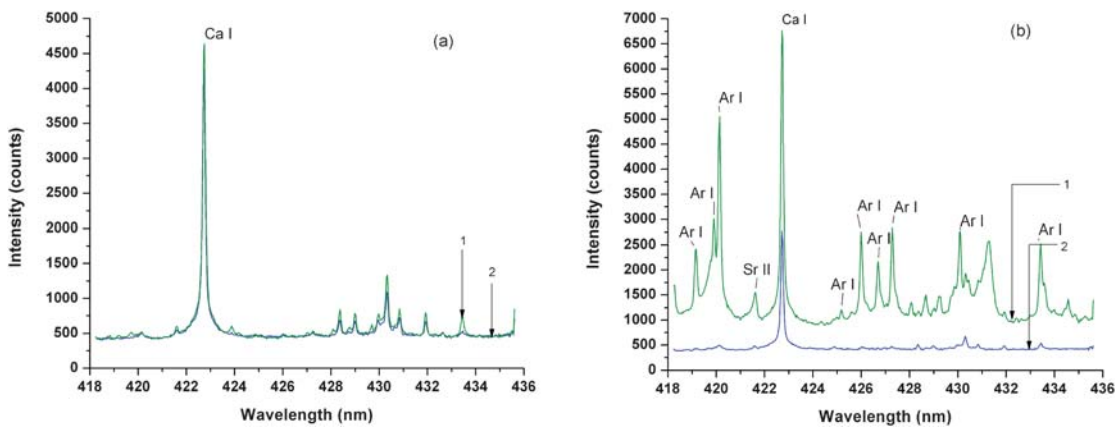

Fig. 8 Alumina spectra in Ar environment: a) 330 MW cm^{-2} on a 0.012 cm^2 spot, b) 15 GW cm^{-2} at focus. (1: microwave ON, 2: microwave OFF.

the argon with and without microwave and a laser irradiance of 330 MW cm^{-2}. No effect of the microwave radiation could be detected. Fig. 8b shows the same spectral region but with laser irradiation of 15 GW cm^{-2} at focus. Enhancement of the signal was detected but emission from Ar lines was predominant causing serious spectral interferences. On the other side, the enhancement of the calcium line was weak (3-fold), as expected based on the study above. For the low irradiance case, the disappearance of the enhancement effect can be explained by the high electron density of laser plasma formed in the Ar. Previous works show that laser-induced plasmas produced in the argon at atmospheric pressure lead to higher electron density than in the air.[21,22] This causes the coupling between the microwave and plasma to be inefficient, similar to the high irradiance case in the air. The breakdown threshold of the alumina sample can not be reached if the irradiance is further decreased. For the high laser irradiance case, the high electron density lowers the breakdown threshold of the argon gas by multiple electron-atom collisions. With the help of large amount of electrons, the microwave is able to generate Ar plasma which gives strong emission enhancement of the Ar lines. Due to the high electron density, the microwave is not able to couple with the plasma efficiently. Therefore the plasma lifetime is short, and the enhancement is weaker than in the air. Because the electron density of the plasma is higher in the Ar than in air, and also noble gas is easier to break down than the air, we don't see air plasma with enhancement of the nitrogen or oxygen lines in the experiments done in normal atmosphere.

Dependence on plasma emitters

The dependence of the enhancement of spectral emission on the excitation level was also observed. Fig. 9 shows seven atomic calcium lines: the $3p^6 4s^2$–$3p^6 4s4p$ transition (E_{up} = 2.9 eV) and the $3p^6 4s4p$–$3p^6 4p^2$ multiplet (E_{up} = 4.8 eV). Other lines were identified to be the second diffraction order of the aluminium lines in the UV. The 422.7 nm line experienced about 22 times enhancement, much stronger enhancement than the neighbouring 428.9 nm calcium line (about 5 times). Higher temperature (reached at early times in the plasma) is needed to support the 428.9 nm transition. Hence, the lifetime of the 428.9 nm radiation is shorter than the 422.7 nm, which leads to weaker enhancement.

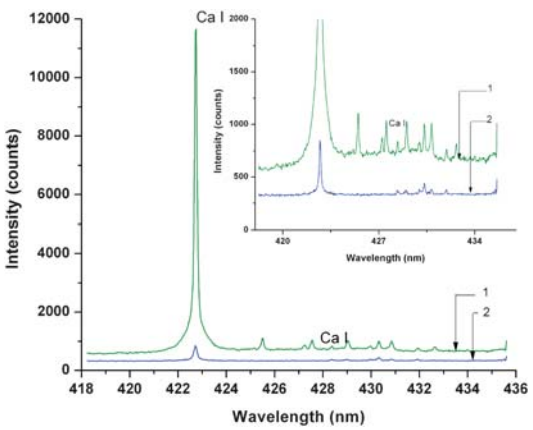

Fig. 9 Enhancement difference between different Ca I excitation levels.

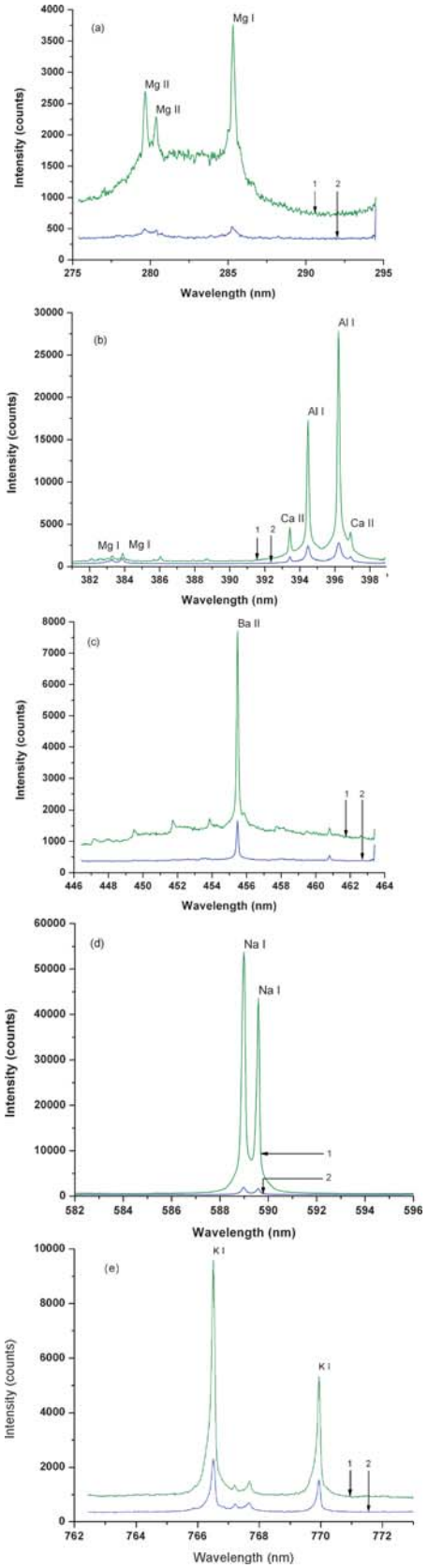

Fig. 10 MA-LIBS spectra for (a) Mg; (b) Al; (c) Ba; (d) Na, and (e) K. (1: MA-LIBS, 2: LIBS).

Table 3 Emission line enhancement summary

Element	Wavelength/nm	Enhancement (times)
Na I	589.6	33
Ca I	422.7	22
Mg I	285.2	16
Al I	396.2	11
Ba II	455.5	5
K I	766.5	5

Similarly, for other elements, most of the lines showing strong enhancement were transitions involving low excitation energy levels, especially resonant lines involving the ground states. Fig. 10 shows the spectra of Al, Mg, Ba, Na, K, and Ca lines with clear intensity enhancement. The enhancement factor varied from 5 to 33, listed in Table 3 for the different elements. Across the spectrum, most of the lines were atomic transitions. Only ionic lines from Mg, Ca, and Ba (atoms of the group II) can be observed due to the combination of low ionization potential (respectively 7.6 eV, 6.1 eV and 5.2 eV) and low ionic excitation energy (respectively 4.4 eV, 3.1 eV and 2.5 eV) as opposed to Na and K (atoms of the group I) that have low ionization potential but have high ionic energy excitation (above 30 eV). The Si, Fe, and Ti lines were weak and difficult to identify in the spectra. As a consequence, the microwave radiation did not generate any noticeable improvement for these elements.

Conclusions

Microwave-Assisted Laser-Induced Breakdown Spectroscopy (MA-LIBS) was systematically evaluated for the first time on a complex alumina sample. Better coupling of the microwave radiation, and enhancement factors, were found for low laser ablation irradiance conditions on large spot areas and in normal atmospheric conditions. The enhancement dependence on elements, ionization states, and upper level energy of the transitions were discussed in a qualitative way. These features seem promising for the development of inexpensive analytical plasma techniques where low power lasers and minimal sample preparation are needed, showing possibilities for lower damage of the sample surface without losing emission using MA-LIBS.

Acknowledgements

The authors thank Dr Philip Efthimion and Dan Hoffman from Envimetrics for their discussions, Dr Michael Sigman for the XRF analysis, Mr. Christopher G. Brown, Mr. Matthew Weidman and Mr. Khan Lim for their helpful discussions. This work is supported by the US ARO-MURI program W911NF-06-1-0446 on "Ultrafast Laser Interaction Processes for LIBS and other Sensing Technologies" and by the State of Florida.

Notes and references

1 J. A. C. Broekaert, *Analytical Atomic Spectrometry with Flames and Plasmas*, Wiley-VCH, Weinheim, 2nd edn, 2005.
2 L. H. J. Lajunen and P. Peramaki, *Spectrochemical Analysis by Atomic Absorption and Emission*, Royal Society of Chemistry, 2nd edn, 2004.
3 Michael Cullen, *Atomic spectroscopy in Elemental Analysis*, CRC Press, 2004.
4 D. Cremers, and L. Radziemski, *Handbook of Laser-Induced Breakdown Spectroscopy*, John Wiley, 2006.
5 A. Miziolek, V. Palleschi, I. Schechter, *Laser Induced Breakdown Spectroscopy*, Cambridge University Press, 2006.
6 V. Juvé, R. Portelli, M. Boueri, M. Baudelet and J. Yu, *Spectrochim. Acta, Part B*, 2008, **63**, 1047.
7 C. López-Moreno, S. Palanco and J. Laserna, *J. Anal. At. Spectrom.*, 2004, **19**, 1479.
8 Y. Dikmelik, C. McEnnis and J. Spicer, *Opt. Express*, 2008, **16**, 5332.
9 W. Schade, C. Bohling, K. Hohmann and D. Scheel, *Laser Part. Beams*, 2006, **24**, 241.
10 A. Sarkar, D. Alamelu and S. Aggarwal, *Talanta*, 2009, **78**, 800.
11 J. Scaffidi, S. Angel and D. Cremers, *Anal. Chem.*, 2006, **78**, 24.
12 V. Babushok, F. DeLucia Jr, J. Gottfried, C. Munson and A. Miziolek, *Spectrochim. Acta, Part B*, 2006, **61**, 999.
13 M. Weidman, S. Palanco, M. Baudelet and Martin C. Richardson, *Spectrochim. Acta, Part B*, 2009, **64**, 961.
14 M. Weidman, M. Baudelet, S. Palanco, M. Sigman, P. Dagdigian and M. Richardson, *Opt. Express*, 2010, **18**, 259.
15 D. K. Killinger, S. D. Allen, R. D. Waterbury, C. Stefano and E. L. Dottery, *Opt. Express*, 2007, **15**, 12905.
16 Y. Ikeda and M. Kaneko, *14th Int. Symp. On Appl. Laser Techniques to Fluid Mechanics*, 2008.
17 B. Kearton and Y. Mattley, *Nat. Photonics*, 2008, **2**, 537.
18 *Envimetrics, LAMPS unit manual*, 2009.
19 Y. Liu, N. Barbieri, M. Weidman, M. Baudelet and M. Richardson, *North-America Symposium on Laser-Induced Breakdown Spectroscopy 2009*, 2009.
20 J. A. Aguilera, C. Aragón and F. Peñalba, *Appl. Surf. Sci.*, 1998, **127–129**, 309–314.
21 L. St-Onge, E. Kwong, M. Sabsabi and E. B. Vadas, *Spectrochim. Acta, Part B*, 2002, **57**, 1131.
22 J. A. Aguilera and C. Aragon, *Appl. Phys. A: Mater. Sci. Process.*, 1999, **69**(7), S475.